Modeling optical effects and thickness dependent current in polymer bulk-heterojunction solar cells

Douglas W. Sievers, Vishal Shrotriya, and Yang Yang[a)]
Department of Materials Science and Engineering, University of California, Los Angeles, Los Angeles, California 90095

(Received 27 April 2006; accepted 19 September 2006; published online 8 December 2006)

Device characteristics of polymer based bulk-heterojunction photovoltaic cells incorporating poly[2-methoxy-5-(2′-ethyl-hexyloxy)-1,4-phenylene vinylene] and methanofullerene ([6,6]-phenyl C_{61}-butyric acid methyl ester) as the active materials are examined as a function of active layer thickness. The dependence of short circuit current on optical effects and its oscillatory variation on the polymer layer thickness is explained by solving the short circuit current using the drift-diffusion equations, where the light intensity calculated from the optical transfer matrix theory is used as the input for optical carrier generation. Furthermore, the effects of polymer layer thickness on other device operation parameters such as open-circuit voltage, fill factor, and series resistivity are measured. Considering the variation of above mentioned parameters, an optimized power conversion efficiency as high as 1.8% (under simulated air mass 1.5 global conditions) was achieved for a device with a polymer layer thickness of 55 nm. © *2006 American Institute of Physics*. [DOI: 10.1063/1.2388854]

I. INTRODUCTION

Polymer based photovoltaic (PV) devices have attracted a lot of attention in the last decade due to their potential for application as flexible, renewable, nonconservative energy sources. Since the discovery of photoinduced charge transfer between organic donors and acceptors, a great effort has been devoted to explore these materials for photovoltaic applications.[1–3] Plastic photovoltaic devices are now considered as promising renewable energy sources that are alternative to their inorganic counterparts, for example, silicon photovoltaic cells.[4] The obvious advantages of these plastic solar cells include, but are not limited to, their mechanical flexibility, light weight, and lower fabrication cost for larger area devices.[3] However, the performance of these devices is limited by several factors. For example, the high energy band gap of the materials used also limits the capability to harvest the photons with lower energy from the sunlight. More importantly, the charge carrier mobility of organic materials is very low. The poor conductivity of organic thin films cuts down the output power efficiency significantly. The highest power conversion efficiency of polymer photovoltaic devices reported so far is based on the bulk-heterojunction concept. For the poly(3-hexylthiophene) based polymer photovoltaic cells highest efficiencies reaching up to 5% have been reported.[5–7] However, for poly(2-methoxy-(2′-ethyl-hexyloxy)-1,4-phenylene (MEH-PPV) and C_{61}-butyric accid methyl ester (PCBM) blends, the highest efficiency reported so far is 2.9%.[8] The bulk heterojunction provides not only high surface contacts for charge separation,[9] but also an interpenetrating network for efficient charge transport. Recently, the progress on polymer solar cells has moved forward on various frontiers, such as transparent and tandem or stacking structures to enhance the efficiency,[10–12] narrow band gap polymers,[13–15] and using triplet compounds[16] as active materials. More importantly, the measurement of organic solar cells, which is not trivial, has been investigated in detail.[17] This standard measurement procedure will make the efficiency measurement procedure for organic solar cells consistent with silicon solar cells.

There have been several efforts to understand the device operation mechanism of polymer PV devices. The effects of variables such as morphology,[18–20] temperature,[21] light intensity,[22] and optical absorption[23,24] on the device performance, and primarily on the short circuit current characteristics, has been studied extensively. However, there has not been any substantial study on the nature of optical effects on short circuit current and their dependence on the thickness of the active polymer layer in PV devices. Optical effects have been studied for bilayer organic solar cells (based on small organic molecules),[25] but the dependence of device operation parameters such as short circuit current on the active layer thickness for polymer-fullerene solar cells has not been studied. Recently, a study on optical effects in polymer-fullerene blend photodiodes was reported but no treatment on recombination and charge transport was included.[26] In this manuscript, we report the optical effects on the short circuit current of polymer-fullerene based bulk-heterojunction PV cells and the effect of active layer (polymer-fullerene blend) thickness on the device performance. We provide a combined framework of optics and charge transport that directly link theoretical and experimental data. The effect of active layer thickness on device parameters such as current, fill factor, and series resistance of the device is reported. An optimum thickness of the active layer was achieved, giving a power conversion efficiency of 1.8%.

II. EXPERIMENTAL

A typical polymer photovoltaic device in this study consisted of a layer of polymer thin film sandwiched between a

a)Electronic mail: yangy@ucla.edu

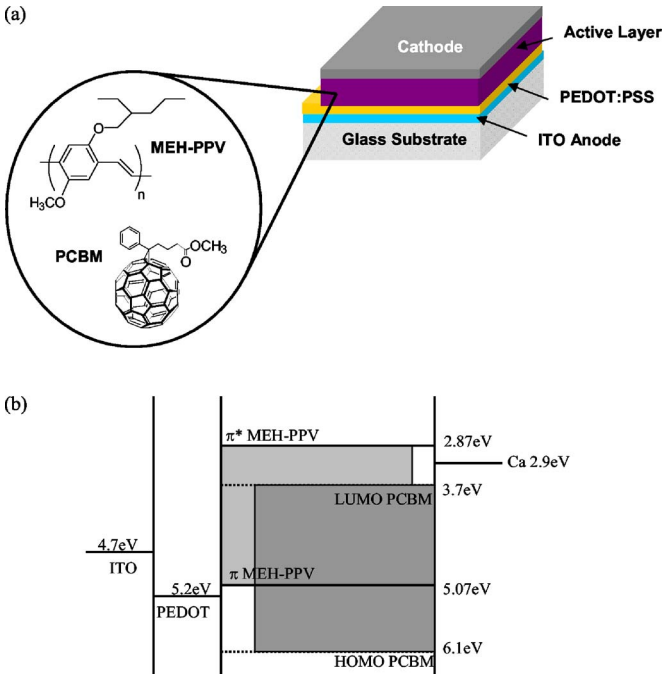

FIG. 1. (a) The device structure of a typical polymer bulk-heterojunciton solar cell fabricated in this study. The chemical structures of MEH-PPV and PCBM are also shown. (b) A schematic showing energy levels of various components in the device structure.

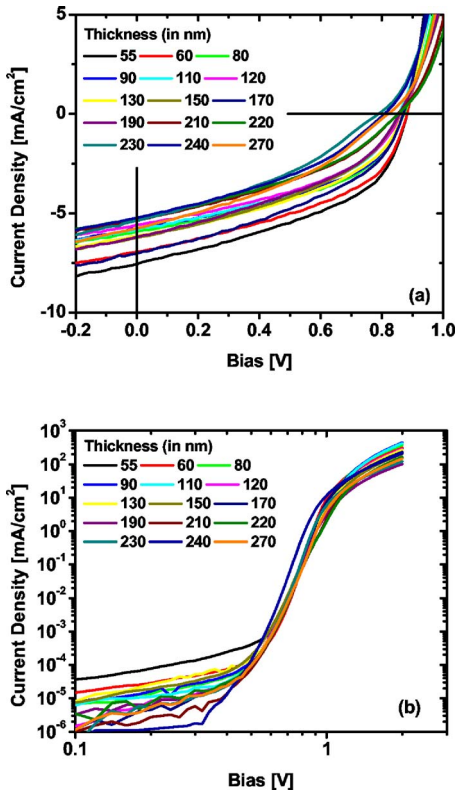

FIG. 2. (Color online) *J-V* characteristics of PV devices as a function of active layer thickness (a) under illumination and (b) in the dark (log-log plot). The illumination was supplied by an Oriel 150 W solar simulator under a simulated 130 mW/cm^2 AM 1.5 G condition.

transparent anode [indium tin oxide (ITO)] and a metal cathode. The active polymeric material is an admixture of MEH-PPV, a *p*-type polymer, and PCBM, an *n*-type acceptor. The ITO glass substrates were cleaned by ultrasonic treatment in detergent, de-ionized water, acetone, and isopropyl alcohol sequentially. The ITO surface was then modified by spin-coating a thin layer (about 25 nm) of poly(3,4-ethylenedioxythiophene) poly(styrenesulfonate) (PEDOT:PSS) (Baytron® P VP Al 4083) from water. This was followed by thermal treatment of the substrates at 120 °C for 2 h. Then, a MEH-PPV and PCBM mixture solution (MEH-PPV:PCBM=1:4 by weight ratio; MEH-PPV concentration=0.7 wt % in 1,2-dichlorobenzene) was spin coated from 1,2-dichlorobenzene on the prepared anodes. The thickness of the polymer films was controlled by changing and optimizing the spinning speeds. Finally, the cathode, consisting of 500 Å of Ca and 800 Å of Al layers, was thermally deposited on the top of the polymer film under vacuum of $\sim 10^{-6}$ Torr. The active area of the device was around 0.12 cm^2. Figure 1 shows the device structure for a typical PV cell fabricated in this study and the energy level diagram under no applied bias. The current-voltage (*J-V*) curves were obtained by a Keithley 2400 source-measure unit. The photocurrent was measured under illumination supplied by a Thermal Oriel 150 *W* solar simulator [air mass 1.5 global (AM 1.5G)]. The thicknesses of the various films were measured using a Dektak profilometer. All devices were fabricated and tested in oxygen and moisture-free nitrogen ambient inside the glovebox.

III. RESULTS AND DISCUSSION

The measured *J-V* characteristics for PV cells with varying thicknesses of active polymer layer are shown in Fig. 2. Figure 2(a) shows the *J-V* curves measured under illumination at a light intensity of 166 mW/cm^2 under simulated AM 1.5G conditions, whereas Fig. 2(b) shows the *J-V* curves in a log-log plot measured under the dark. The thickness of the active layer, which comprised of MEH-PPV and PCBM blended together in the 1:4 weight ratio, was varied from 55 to 270 nm by varying the spinning speed during spin casting of the active layer from solution. As seen from the figures, the *J-V* characteristics under illumination change considerably on varying the thickness. For devices with active layer thickness of only 55 nm, the short circuit current (J_{SC}) was the highest, 7.55 mA/cm^2, whereas it was significantly lower for the device with active layer thickness of 270 nm, being only 5.75 mA/cm^2. The variation of J_{SC} with the thickness of the active layer is plotted in Fig. 3. There are two noticeable variations in the curve that fits the data points over the range of thicknesses. Firstly, there is an oscillatory variation in the value of J_{SC} as the thickness increases, and secondly, there is an overall decrease in the value that gives the shape of the curve a gradually declining oscillatory variation.

In photovoltaics, the short circuit current is due to light absorption; thus the oscillatory nature of the short circuit current is very likely due to an optical effect. To determine the validity of this statement, we have modeled the variation in light intensity throughout the device, which allows the distribution of photogenerated carriers to be determined. For layers that are similar in thickness to the wavelength of light in the material, it is necessary to include interference effects

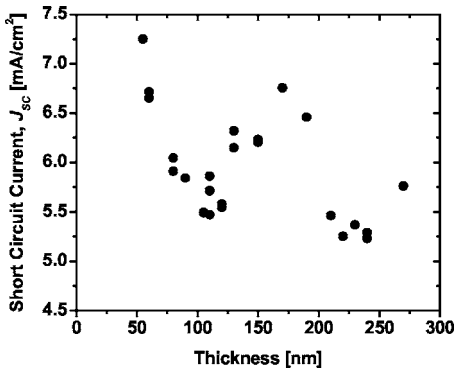

FIG. 3. Measured values of short circuit current density (J_{SC}) in mA/cm^2 as a function of active layer thicknesses given in nanometers as obtained from *J-V* curves shown in Fig. 2(a).

in the calculation. Here we apply the optical transfer-matrix theory introduced by Heavens,[27] which was more recently applied to organic heterojunction solar cells by Pettersson *et al.*[28].

In the optical transfer-matrix theory, light is considered as a plane wave. For photovoltaic devices, we will only consider light at normal incidence to the substrate. The electric field of the light at any point in the device is a complex quantity and is given a positive superscript $E^+(x)$ for waves traveling from left to right and a negative superscript $E^-(x)$ for waves traveling from right to left, as shown in Fig. 4. The device consists of a stack of m layers, each of which is described by its complex index of refraction $\tilde{n}=n+i\kappa$ and thickness d, sandwiched between the glass substrate and the atmosphere. The behavior of light at the interface between two layers, j and k, can be described by a 2×2 matrix that contains the complex Fresnel coefficients. This matrix $\mathbf{I}_{jk}$ is known as the interface matrix, which for normal incidence can be given in the simplified form

$$\mathbf{I}_{jk}=\begin{bmatrix}(\tilde{n}_j+\tilde{n}_k)/2\tilde{n}_j & (\tilde{n}_j-\tilde{n}_k)/2\tilde{n}_j\\ (\tilde{n}_j-\tilde{n}_k)/2\tilde{n}_j & (\tilde{n}_j+\tilde{n}_k)/2\tilde{n}_j\end{bmatrix}. \tag{1}$$

Similarly, the effect on the electric field from propagating through each layer is described by a 2×2 matrix $\mathbf{L}_j$ known as the layer matrix

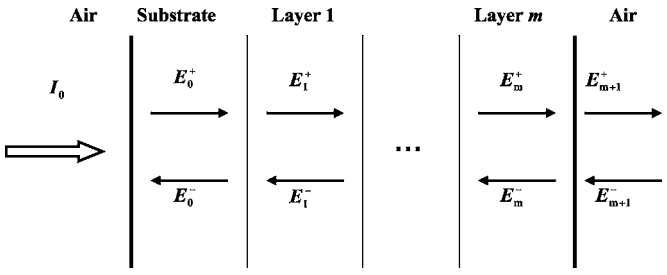

FIG. 4. The solar cell consists of a stack of m thin-film layers sandwiched between air and a semi-infinite substrate. Solar radiation is incident on the substrate from the left, with intensity I_0 for each wavelength in the AM 1.5 G spectrum. The electric field of waves traveling to the right are denoted as E^+; those traveling left E^-. The substrate and air at the back of the device are treated as layers 0 and $m+1$, respectively.

$$\mathbf{L}_j=\begin{bmatrix}e^{-i\xi_j d_j} & 0\\ 0 & e^{i\xi_j d_j}\end{bmatrix}, \tag{2}$$

where $\xi_j=2\pi\tilde{n}_j/\lambda$ and λ is the wavelength of the light. The components of the optical electric field within the substrate (subscript 0) are related to those in the atmosphere (subscript $m+1$) by the total transfer matrix $\mathbf{S}$

$$\begin{bmatrix}E_0^+\\ E_0^-\end{bmatrix}=\mathbf{S}\begin{bmatrix}E_{m+1}^+\\ E_{m+1}^-\end{bmatrix}, \tag{3}$$

where $\mathbf{S}$ is the product of all interface and layer matrices

$$\mathbf{S}=\begin{bmatrix}S_{11} & S_{12}\\ S_{21} & S_{22}\end{bmatrix}=\left(\prod_{\nu=1}^{m}\mathbf{I}_{(\nu-1)\nu}\mathbf{L}_\nu\right)\mathbf{I}_{m(m+1)}. \tag{4}$$

The field quantities in Eq. (3) are those that exist at the boundaries with the stack of m layers that makes up the active part of the device. Considering light incident from the substrate side only requires that $E_{m+1}^-=0$, allowing the reflection and transmission coefficients of the multilayer stack to be expressed as

$$r=S_{21}/S_{11} \tag{5a}$$

$$t=1/S_{11}. \tag{5b}$$

To determine the electric field at a distance x within layer j of the device, one must add the left- and right-traveling waves,

$$E_j(x)=E_j^+(x)+E_j^-(x). \tag{6}$$

To find these two latter quantities, Eq. (4) is split into two partial transfer matrices by the relation $\mathbf{S}=\mathbf{S}_j'\mathbf{L}_j\mathbf{S}_j''$. These two matrices are separately defined as

$$\mathbf{S}_j'=\begin{bmatrix}S_{j11}' & S_{j12}'\\ S_{j21}' & S_{j22}'\end{bmatrix}=\left(\prod_{\nu=1}^{j-1}\mathbf{I}_{(\nu-1)\nu}\mathbf{L}_\nu\right)\mathbf{I}_{m(m+1)}, \tag{7a}$$

$$\mathbf{S}_j''=\begin{bmatrix}S_{j11}'' & S_{j12}''\\ S_{j21}'' & S_{j22}''\end{bmatrix}=\left(\prod_{\nu=j+1}^{m}\mathbf{I}_{(\nu-1)\nu}\mathbf{L}_\nu\right)\mathbf{I}_{m(m+1)}. \tag{7b}$$

Algebraic manipulation then allows Eq. (6) to be expressed in terms of known quantities,

$$E_j(x)=t_j^+[e^{i\xi_j x}+r_j''e^{i\xi_j(2d_j-x)}]E_0^+, \tag{8}$$

where E_0^+ is the electric field inside the substrate incident on layer 1,

$$t_j^+=[S_{j11}'+S_{j12}'r_j''e^{2i\xi_j d_j}]^{-1} \tag{9}$$

and

$$r_j''=S_{j21}''/S_{j11}''. \tag{10}$$

Due to the large thickness of the glass ($\sim$1.0 mm), the substrate cannot be included directly in the transfer-matrix calculation. However, to obtain quantitatively accurate results for the intensity in each layer, the effect of the substrate is included by summing the intensities within the glass as opposed to the electric fields. The intensity of light incident on the multilayer from within the substrate I_S is then given by

$$I_S = I_0 \frac{T_S e^{-\alpha_S d_S}}{1 - R R_S e^{-2\alpha_S d_S}} = I_0 T_{\text{int}}, \tag{11}$$

where I_0 is the light intensity incident on the device, R and T are the reflectance and transmittance of the multilayer stack, and variables subscripted with S represent values for the substrate. This allows us to define an internal transmittance T_{int} for the substrate in terms of the absorption coefficient $\alpha_j = 4\pi\kappa_j/\lambda$. By combining Eqs. (8) and (11), the light intensity at a distance x within layer j of the device can be expressed as

$$I_j(x) = I_0 T_{\text{int}} |t_j^+|^2 \, \text{Re}\left(\frac{\tilde{n}_j}{\tilde{n}_s}\right)\{e^{-\alpha_j x} + \rho_j''^2 e^{-\alpha_j(2d_j - x)} + 2\rho_j'' e^{-\alpha_j d_j} \cos[4\pi n_j(d_j - x)/\lambda + \delta_j'']\}, \tag{12}$$

where ρ_j'' is the argument and δ_j'' is the phase of the quantity in Eq. (10). Using this equation, the intensity at every point in the device can be calculated. Readers interested in a more thorough derivation are referred to Ref. 28.

Once the light intensity profile in the active layer is known, the rate of energy dissipated per unit volume Q can be determined by $Q(x,\lambda) = \alpha(\lambda) I(x,\lambda)$. Assuming a photon to exciton conversion efficiency of η, the exciton generation rate X can be expressed by dividing Q by the energy of a single photon of wavelength λ and integrating over all wavelengths in the spectrum, or

$$X(x) = \eta \int_{350}^{800} \frac{\lambda}{hc} Q(x,\lambda) d\lambda, \tag{13}$$

where h and c are Planck's constant and the speed of light in vacuum. The electron transfer from polymer to PCBM is very fast;[9] therefore a value of $\eta = 1$ is assumed. Here the integration is performed from 350 to 800 nm, which is appropriate because the glass absorbs strongly below 350 nm and neither MEH-PPV nor PCBM absorbs appreciably beyond 800 nm.

In studying the effects of thickness, it is understood that the built-in electric field will change with the thickness. However, the field dependence of the probability for exciton dissociation into free charge carriers in organic solar cells has only more recently been taken into consideration.[29,30] The theory of geminate recombination, originally described by Onsager[31] and later extended by Braun,[32] proposes that the probability of exciton dissociation is distance, field, and temperature dependent,

$$p(x,F,T) = \frac{k_d(x,F,T)}{k_d(x,F,T) + k_r}, \tag{14}$$

where x is the distance between the bound charges of the exciton, F is the electric field, T is the temperature, k_r is the rate at which excitons relax to the ground state, and k_d is the dissociation rate

$$k_d(x,F,T) = \frac{3\gamma}{4\pi x^3} e^{-U_b/k_B T} \frac{J_1(2\sqrt{-2b})}{\sqrt{-2b}}. \tag{15}$$

In this expression γ is the Langevin bimolecular recombination rate constant, $U_b = q^2/(4\pi\varepsilon_r\varepsilon_0 x)$ is the exciton binding energy, J_1 is the first order Bessel function, and the field parameter $b = q^3 F/(8\pi\varepsilon_r k_B^2 T^2)$. These expressions also include the electronic charge q, the material's dielectric constant ε_r, the permittivity of free space ε_0, and Boltzmann's constant k_B. In disordered polymer systems, it is appropriate to treat the charge-separation distance not as a constant, but instead as a distribution of distances. A spherically averaged Gaussian distribution has been shown to be most appropriate,[33] for which the overall exciton dissociation probability becomes an integral over all charge-separation distances

$$P(F,T) = \frac{4}{\sqrt{\pi} a^3} \int_0^\infty p(x,F,T) x^2 e^{-(x/a)^2} dx, \tag{16}$$

where a is the charge-separation distance at which the probability of the Gaussian function is a maximum.

To determine the steady-state short circuit current of the solar cell, we solve the continuity equations using a drift-diffusion expression for the current, which are coupled to Poisson's equation

$$\frac{\partial n}{\partial t} - \frac{1}{q}\frac{\partial J_n}{\partial x} = PX - (1-P)R, \tag{17a}$$

$$\frac{\partial p}{\partial t} + \frac{1}{q}\frac{\partial J_p}{\partial x} = PX - (1-P)R, \tag{17b}$$

$$J_n = q\mu_n\left(nF + \frac{k_B T}{q}\frac{\partial n}{\partial x}\right), \tag{17c}$$

$$J_p = q\mu_p\left(pF - \frac{k_B T}{q}\frac{\partial p}{\partial x}\right), \tag{17d}$$

$$\frac{\partial^2 \phi}{\partial x^2} = \frac{q}{\varepsilon_r\varepsilon_0}(p - n). \tag{17e}$$

In the above equations $n(p)$ represents the electron(hole) density, $J_n(J_p)$ the electron(hole) current density, $\mu_n(\mu_p)$ the electron(hole) mobility, and ϕ the electric potential. Due to the finite probability of exciton dissociation the continuity equations take on a slightly modified form,[30] where the generation rate G is replaced by the product PX and the recombination rate is multiplied by $(1-P)$.

The equilibrium solution is found first by solving Poisson's equation using a finite-difference method, where the electron and hole densities are defined in terms of the electric potential,

$$n = N_C e^{-(E_C - q\phi - \varphi)/k_B T}, \tag{18a}$$

$$p = N_V e^{(E_V - q\phi - \varphi)/k_B T}, \tag{18b}$$

where $N_C(N_V)$ is the effective density of states for electrons(holes), $E_C(E_V)$ is the electron(hole) transport level, and ψ is the Fermi energy. The steady-state solutions are then found by integrating the equilibrium solution forward in time using the time-evolution method of Davids *et al.*[34] which uses an additional equation for the time derivative of the electric field

$$\frac{\partial F}{\partial t} = -\frac{1}{\varepsilon_r \varepsilon_0}\left(J(x) - \frac{1}{L}\int_0^L J(x)dx\right), \tag{19}$$

where L is the thickness of the active polymer layer. Recombination is assumed to be of the Langevin bimolecular form

$$R = \gamma(np - n_i^2), \tag{20}$$

where the recombination rate constant is defined as $\gamma = q(\mu_n + \mu_p)/\varepsilon_r\varepsilon_0$ and the intrinsic carrier density is given as

$$n_i = \sqrt{N_C N_V} e^{-E_g/2k_BT}. \tag{21}$$

Because the built-in electric field will change with thickness, the field dependence of the carrier mobility is taken into account by using the Frenkel-Poole form $\mu = \mu_0 e^{\sqrt{F/F_0}}$. Both the mobilities and exciton dissociation probabilities are calculated from the average electric field in the device, rather than at each point, to enhance the speed of the simulation.

A proper solution of the problem also requires the appropriate boundary conditions. Because the work function of PEDOT:PSS lies below the MEH-PPV highest occupied molecular orbital (HOMO) and similarly the work function of Ca lies above the PCBM lowest unoccupied molecular orbital (LUMO), Ohmic boundary conditions are assumed. At the PEDOT:PSS contact, defined as $x=0$, this implies

$$p(0) = N_V, \tag{22a}$$

$$n(0) = N_C e^{-E_g/k_BT}, \tag{22b}$$

and similarly at the Ca contact, where $x=L$,

$$n(L) = N_C, \tag{23a}$$

$$p(L) = N_V e^{-E_g/k_BT}. \tag{23b}$$

The final two boundary conditions are on the electric potential, which for the short circuit condition is $\phi(0) = \phi(L) = 0$.

Many parameters are necessary as inputs to the model. The index of refraction (n) and extinction coefficient (κ) data for calculating the exciton generation rate used were obtained from several sources; those of calcium were obtained from Ref. 35, and the data for MEH-PPV were assumed similar to those of MDMO-PPV, for which the data in Ref. 36 were used. For the glass, ITO, PEDOT, and aluminum layers, data were obtained from the authors of Ref. 28. The light intensity spectrum [$I_0(\lambda)$ vs λ, where $I_0(\lambda)$ is the spectral irradiance of the solar simulator in W m^{-2} μm^{-1} and λ is the wavelength in nanometers], obtained from Thermal Oriel, was described as a typical spectrum, and was scaled appropriately to achieve an intensity of 166 mW/cm^2. The remaining parameters, which were adjusted to best fit the measured J_{SC} data, are listed in Table I.

Figure 5 shows the measured short circuit current density as a function of active layer thickness, along with that calculated using the model. As can be seen from the comparison, the prominent features of the experimental data are reproduced well by the model. The oscillatory nature of the short circuit current exists both in the model calculation and the experimental data, although the relative extrema predicted by the model are shifted to slightly larger thicknesses. We believe that a more rigorous fitting of the parameters would bring the theoretical and experimental curves in closer agreement, especially by using more accurate optical data. Such data, as obtained by ellipsometry, are currently beyond our limitations.

TABLE I. The quantities used in fitting the model to the data, as shown in Fig. 5.

Quantity	Symbol	Value
Dielectric constant	ε_r	3.4
Relaxation rate	k_r	5×10^6 s^{-1}
Most probable exciton charge-separation distance	a	1.3 nm
Electron transport level (PCBM LUMO)	E_C	3.7 eV
Electron effective density of states	N_C	5.3×10^{25} m^{-3}
Hole transport level (MEH-PPV HOMO)	E_V	5.07 eV
Hole effective density of states	N_V	4.2×10^{25} m^{-3}
Electron zero-field mobility	$\mu_{n,0}$	7.0×10^{-8} m^2/V s
Electron Frenkel-Poole field parameter	$F_{n,0}$	1.0×10^9 V/m
Hole zero-field mobility	$\mu_{p,0}$	9.0×10^{-9} m^2/V s
Hole Frenkel-Poole field parameter	$F_{p,0}$	4.0×10^7 V/m

To further understand the nature of the oscillatory behavior, we have also calculated the short circuit current using two different models. First, we use the common assumption that the light intensity decays exponentially as it travels through the polymer film. This assumption is employed by many of the models reviewed by Harrison *et al.*[37] In these calculations, the initial light intensity in the polymer film is calculated by using the transmittance from the air into the MEH-PPV:PCBM film, where the transmittance of the glass/ITO/PEDOT:PSS structure is determined using the optical multilayer theory. This description gives the most accurate comparison with the previously outlined model (model 1). As shown in Fig. 6, the model using exponential decay (model 2) can describe neither the oscillations in current nor its decrease at larger thicknesses.

A second variation in the model was also investigated, in which the original light intensity profile described (model 1) was used, but all excitons are assumed to be dissociated. In this model, the right-hand side of Eq. (17) is replaced with the more standard form $X-R$. As shown in Fig. 6, ignoring

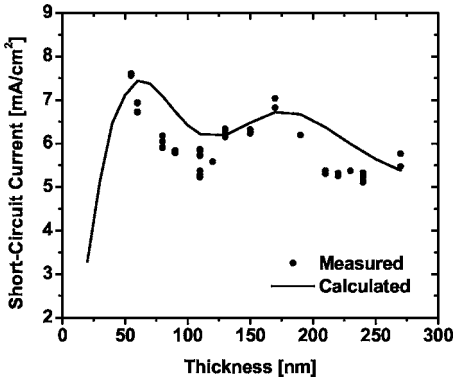

FIG. 5. A comparison of the measured and calculated short circuit current density (J_{SC}) in mA/cm^2 as a function of active layer thickness given in nanometers. The solid circles represent the data measured from the J-V curves under illumination shown in Fig. 2(a). The solid curve represents the data calculated from the model.

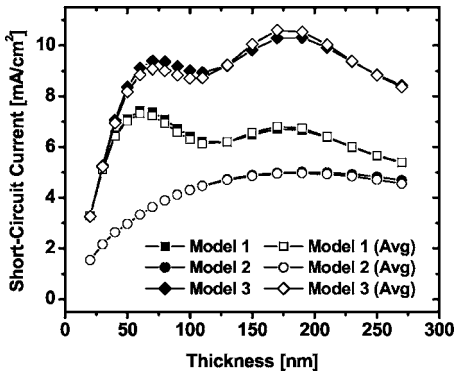

FIG. 6. A comparison between the different models investigated. Model 1 includes optical interference by the transfer-matrix theory as well the exciton dissociation probability. Model 2 ignores optical interference and assumes exponential decay of light intensity, with exciton dissociation probability included. Model 3 includes optical interference but assumes that all excitons are dissociated. Curves marked with (Avg) denote the same model using the averaged value for the optical exciton generation rate

the dissociation probability greatly overestimates the short circuit current for thicknesses of 50 nm and above (model 3). However, the positions of the minima and maxima versus thickness agree well, which reinforces our hypothesis that optical effects dominate the oscillatory behavior in the short circuit current. To summarize the three model we have used model 1 includes optical interference by the transfer-matrix theory as well the exciton dissociation probability, model 2 ignores optical interference and assumes exponential decay of light intensity, with exciton dissociation probability included, and model 3 includes optical interference, but assumes all excitons are dissociated.

Another interesting observation can be made by looking at Fig. 6. For each of the models described, the currents were calculated using the averaged exciton generation rate $\overline{X(x)}$. These plots, followed by (Avg) in the legend, are strikingly similar to those in which the full position dependence of X is used. This suggests that the relative positions of intensity minima and maxima are not important in this material system, but the mean level of the intensity is. Such is not true for bilayer heterojunctions, where the position of the maximum light intensity has a large impact on device performance.[28]

Figures 7(a) and 7(b) show the variation of fill factor (FF) and the series resistance (R_S), respectively, of the PV cells with the thickness of the active layer. The fill factor of solar cells is given as $\mathrm{FF}=I_{\max}V_{\max}/I_{\mathrm{SC}}V_{\mathrm{OC}}$, where $I_{\max}$ and $V_{\max}$ are the current and voltage at the maximum power point of the I-V curve in the fourth quadrant. A large serial resistance in the equivalent circuit of the solar cell can result in a reduced value of FF. From Fig. 7(b), it can be seen that the value of R_S increases almost linearly with the thickness of the active layer. The resistance R_S was calculated using the equivalent circuit described in Ref. 4, from the log dark current density versus voltage curves shown in Fig. 2(b) by using the equation $R_S=\Delta V/I$, where ΔV is the voltage offset from linearity at high bias and I is the current. One of the major factors that contribute to series resistance is the resistivity of the bulk layer, and thus with the increasing thickness of the active layer, the observed linear increase of R_S is understandable. As a result of this increase in the R_S, the FF decreases linearly with the increasing thickness of the active layer as shown in Fig. 7(a). The above results for FF and R_S are in good agreement with the results reported previously,[38] although much thinner active layers have also been considered in this study. Also from Fig. 2(a), V_{OC} of the PV cells remains almost constant and is independent of the thickness of the polymer layer. This is not surprising as it has been reported previously that the V_{OC} depends mostly on the energy levels of the electron donor and acceptor system, which in our study remains the same for all the devices. The power conversion efficiency of the solar cell is calculated from $\eta_{\mathrm{eff}}=V_{\mathrm{OC}}J_{\mathrm{SC}}\mathrm{FF}/I_{\mathrm{light}}$, where V_{OC} (measured in volts), J_{SC} (measured in $\mathrm{mA/cm^2}$), and FF are as described above and I_{light} is the incident solar radiation in $\mathrm{mW/cm^2}$. Figure 8 shows η_{eff} as a function of the active layer thickness. The polynomial fit to the experimental data shown represents a guide to the eye, rather than model results. The incident light intensity remains the same for all the devices, and therefore the efficiency will depend on the product of FF, J_{SC}, and V_{OC}, as is visible from Fig. 8, where the variation in η_{eff} can be thought of as the superimposition of curves in Figs. 3 and 7(a). The oscillatory dependence of the curve on thickness is because of a similar oscillatory dependence of J_{SC} on the thickness as explained above. Here we have noted that the optimal thickness that we have obtained for best performance of our devices is ~55 nm. However, we have reported experimental results for devices with minimum active

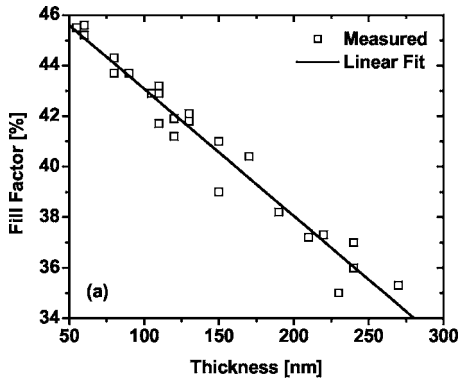

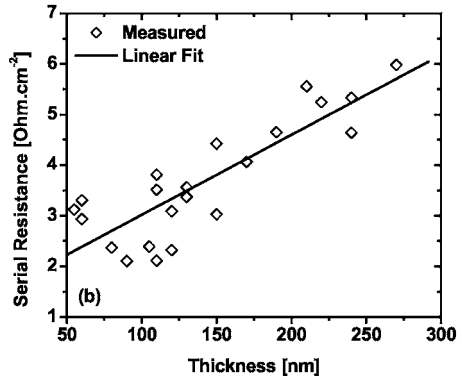

FIG. 7. Measured values of (a) fill factor and (b) serial resistivity of polymer solar cells as functions of active layer thickness. The linear fit to the measured data is shown by the solid lines. The series resistance was calculated from the dark J-V characteristics shown in Fig. 2(b) from the relation $R_S=\Delta V/I$.

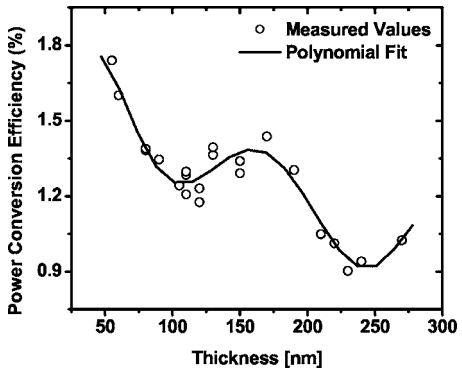

FIG. 8. Measured power conversion efficiency (in percent) as a function of active layer thickness for the solar cells. The polynomial fit to the experimental data shown represents a guide to the eye, rather than model results.

layer thickness of only 55 nm. One of the primary reasons for not including results for devices with thinner active layers is that the quality of the film is very poor when spin cast at the very high speeds required to obtain a thin film. Such films have pin holes and other defects along with a nonuniform surface, which have an adverse effect on the performance of the device. Therefore, the proposed model may not provide an accurate description of the measured current-voltage characteristics for devices with a thickness below 55 nm due to the increased leakage current in devices with such defects. However, we believe that if thinner defect-free films can be obtained with sufficient uniformity, the model will provide an accurate agreement to the *I-V* characteristics for such devices as well.

IV. CONCLUSION

In conclusion, we studied the effect of active layer thickness on the electrical characteristics of the photovoltaic devices and presented a model to explain the effect of thickness on the optical absorption and thus the short circuit current in the PV cells. A gradually declining oscillatory dependence of power conversion efficiency on the active layer thickness was observed and explained on the basis of the effect on FF, J_{SC}, and V_{OC} of the device as the thickness is varied. Model calculations and the experimental results suggested that for an optimum thickness of the active layer, the highest power conversion efficiency can be obtained close to 55 nm, which in this study was close to 1.8%.

ACKNOWLEDGMENTS

This work was supported in part by the NSF IGERT: Materials Creation Training Program (MCTP) (DGE-0114443), the Office of Naval Research (N00014-01-1-0136, program manager Dr. Paul Armistead), and the Air Force Office of Scientific Research (F49620-03-1-0101, program manager Dr. Charles Lee). The authors would like to thank Dr. Chia-Hsun Chen, Dr. Gang Li, and Dr. Jianyong Ouyang for valuable technical discussions.

[1] N. S. Sariciftci, L. Smilowitz, A. J. Heeger, and F. Wudl, Science **258**, 1474 (1992).
[2] G. Yu, J. Gao, J. C. Hummelen, F. Wudl, and A. J. Heeger, Science **270**, 1789 (1995).
[3] C. J. Brabec, N. S. Sariciftci, and J. C. Hummelen, Adv. Funct. Mater. **11**, 15 (2001).
[4] W. D. Johnston, Jr., *Solar Voltaic Cells* (Dekker, New York, 1980).
[5] G. Li, V. Shrotriya, J. Huang, Y. Yao, T. Moriarty, K. Emery, and Y. Yang, Nat. Mater. **4**, 864 (2005).
[6] M. Reyes-Reyes, K. Kim, and D. L. Carroll, Appl. Phys. Lett. **87**, 083506 (2005).
[7] W. L. Ma, C. Y. Yang, X. Gong, K. Lee, and A. J. Heeger, Adv. Funct. Mater. **15**, 1617 (2005).
[8] S. Alem, R. de Bettignies, and J.-M. Nunzi, Appl. Phys. Lett. **84**, 2178 (2004).
[9] B. Kraabel, J. C. Hummelen, D. Vacar, D. Moses, N. S. Sacriciftci, A. J. Heeger, and F. Wudl, J. Chem. Phys. **104**, 4267 (1996).
[10] V. Shrotriya, E. H. Wu, G. Li, and Y. Yang, Appl. Phys. Lett. **88**, 064104 (2006).
[11] G. Li, C.-W. Chu, V. Shrotriya, J. Huang, and Y. Yang, Appl. Phys. Lett. **88**, 253503 (2006).
[12] A. Hadipour *et al.*, Adv. Funct. Mater. **16**, 1897 (2006).
[13] F. Zhang *et al.*, Adv. Funct. Mater. **16**, 667 (2006).
[14] M. M. Wienk, M. G. R. Turbiez, M. P. Struijk, M. Fonrodona, and R. A. J. Janssen, Appl. Phys. Lett. **88**, 153511 (2006).
[15] Y. Yao, C. Shi, G. Li, V. Shrotriya, Q. Pei, and Y. Yang, Appl. Phys. Lett. **89**, 153507 (2006).
[16] Y. Shao and Y. Yang, Adv. Mater. (Weinheim, Ger.) **17**, 2841 (2005).
[17] V. Shrotriya, G. Li, Y. Yao, T. Moriarty, K. Emery, and Y. Yang, Adv. Funct. Mater. **16**, 2016 (2006).
[18] J. Liu, Y. Shi, and Y. Yang, Adv. Funct. Mater. **11**, 420 (2001).
[19] D. Gebeyehu, C. J. Brabec, F. Padinger, T. Fromherz, J. C. Hummelen, D. Badt, H. Schindler, and N. S. Sariciftci, Synth. Met. **118**, 1 (2001).
[20] J. K. J. van Duren, X. Yang, J. Loos, C. W. T. Bulle-Lieuwma, A. B. Sieval, J. C. Hummelen, and R. A. J. Janssen, Adv. Funct. Mater. **14**, 425 (2004).
[21] E. A. Katz *et al.*, J. Appl. Phys. **90**, 5343 (2001).
[22] P. Schilinsky, C. Waldauf, J. Hauch, and C. J. Brabec, J. Appl. Phys. **95**, 2816 (2004).
[23] H. Hoppe, N. Arnold, N. S. Sariciftci, and D. Meissner, Sol. Energy Mater. Sol. Cells **80**, 105 (2003).
[24] H. Hoppe, N. Arnold, D. Meissner, and N. S. Sariciftci, Thin Solid Films **451–452**, 589 (2004).
[25] P. Peumans, A. Yakimov, and S. R. Forrest, J. Appl. Phys. **93**, 3693 (2003).
[26] N.-K. Persson, H. Arwin, and O. Inganas, J. Appl. Phys. **97**, 034503 (2005).
[27] O. S. Heavens, *Optical Properties of Thin Solid Films* (Dover, New York, 1965).
[28] L. A. A. Pettersson, L. S. Roman, and O. Inganäs, J. Appl. Phys. **86**, 487 (1999).
[29] V. D. Mihailetchi, L. J. A. Koster, J. C. Hummelen, and P. W. B. Blom, Phys. Rev. Lett. **93**, 216601 (2004).
[30] L. J. A. Koster, E. C. P. Smits, V. D. Mihailetchi, and P. W. M. Blom, Phys. Rev. B **72**, 085205 (2005).
[31] L. Onsager, Phys. Rev. **54**, 554 (1938).
[32] C. L. Braun, J. Chem. Phys. **80**, 4157 (1984).
[33] T. E. Goliber and J. H. Perlstein, J. Chem. Phys. **80**, 4162 (1984).
[34] P. S. Davids, I. H. Campbell, and D. L. Smith, J. Appl. Phys. **82**, 6319 (1997).
[35] C. M. Ramsdale and N. C. Greenham, J. Phys. D **36**, L29 (2003).
[36] H. Hoppe, N. S. Sariciftci, and D. Meissner, Mol. Cryst. Liq. Cryst. Sci. Technol., Sect. A **385**, 233 (2002).
[37] M. G. Harrison, J. Grüner, and G. C. W. Spencer, Phys. Rev. B **55**, 7831 (1997).
[38] T. Aernouts, W. Geens, J. Poortmans, P. Heremans, S. Borghs, and R. Mertens, Thin Solid Films **403–404**, 297 (2002).